Abbreviations

%N	percentage nitrogen by mass
2-NDPA	2-Nitrodiphenylamine
AIMD	*ab initio* molecular dynamics
AO	atomic orbital
a.u.	atomic units
B3LYP	Becke, 3-parameter, Lee-Yang-Parr hybrid functional
BCP	bonding critical point
BSSE	basis set superposition error
CH_3/CH_3	NC repeat unit with two $-OCH_3$ capping groups
CH_3/OH	NC repeat unit with $-OCH_3$ capping group on ring 1 and $-OH$ group on ring 2
OH/CH_3	NC repeat unit with $-OH$ capping group on ring 1 and $-OCH_3$ group on ring 2
CCP	cage critical point
CP	critical point
DFT	density functional theory
DFT-D	density functional theory with dispersion correction
DSC	differential scanning calorimetry
DOS	degree of substitution

DPA diphenylamine

EN ethyl nitrate

ESP electrostatic potential

G09 Gaussian 09 revision E.01

GGA generalised gradient approximation

GM genetically modified

GTO Gaussian type orbitals

GView Gauss View 5.0.8

HF Hartree-Fock

HMF hydroxymethylfurfural

HOMO highest occupied molecular orbital

IR infra-red spectroscopy

KS-DFT Kohn-Sham DFT

LDA local density approximation

MD molecular dynamics

MEP minimum energy path

MM molecular mechanics

MMFF94 Merck molecular force field 94

MO molecular orbitals

MP2 Møller–Plesset perturbation theory with second order correction

MW molecular weight

NBO natural bond orbital

NC nitrocellulose

NCP nuclear critical point

NG nitroglycerine

NMR nuclear magnetic resonance spectroscopy

PCM polarisable continuum model

PES potential energy surface

PETN pentaerythritol tetranitrate

PETRIN pentaerythritol trinitrate

QM quantum mechanics

QTAIM quantum theory of atoms in molecules

RCP ring critical point

RESP restrained electrostatic potential atomic partial charges

RHF restricted HF

RMS root mean square

ROHF restricted-open HF

UHF unrestricted HF

SB59 1,4-bis(ethylamino)-9,10-anthraquinone dye

SCF self-consistent field

SEM scanning electron microscopy

SMD solvation model based on density

S_N2 bi-molecular nucleophilic substitution reaction

STO Slater type orbitals

TG thermogravitmetric analysis

TS transition state

UFF	universal force field
UV	ultraviolet
UV-vis	ultraviolet–visible spectroscopy
vdW	van der Waals
ωB97X-D	ωB97X-D long-range corrected hybrid functional
ZPE	zero-point energy

Chapter 1

Post-Denitration Reactions

1.1 Introduction

Products of the preliminary denitration step of **NC!** (**NC!**) can be evolved as gases or remain trapped in the polymer matrix. Reactive nitrogen dioxide radicals generated from homolysis of the O-N bond are likely to migrate within the bulk and attack other sites on the polysaccharide, initiating branched radical chain reactions. These lead to deeper decomposition of the polymer *via* chain scission and rupture of glucose rings, with eventual complete disintegration of the molecule, assisted by products released by ongoing acid hydrolysis. Nitrous and nitric acids are released directly from denitration or via transformation of released NO_x species. In addition to catalysing hydrolysis, they increase the acidity of the overall system, lowering the pH and stimulating further hydrolytic processes [**?**]. The final product mixture is dictated by the numerous side reactions involving autocatalysis, radical reactions and product interactions.

When studying the ageing of **NC!** using ultraviolet–visible spectroscopy, Moniruzzaman *et al.* observed increasing concentrations of reaction products beyond those generated from first-stage decomposition, following heat treatment over extended timescales [**?**, **?**]. The reaction of the 1,4-bis(ethylamino)-9,10-anthraquinone (**SB59!** (**SB59!**)) with NO_x released by denitration, mimics the action of stabilisers such as **DPA!** (**DPA!**) and **2NDPA!** (**2NDPA!**) commonly used in **NC!** formulations (figure **??**). The secondary amine groups of the dye consume any nitrates in the system, eliminating the possibility of successive reactions generating acidic species. Un-aged **NC!** thin films, and films aged at 40°C, 50°C, 60°C and 70°C for timescales of up to 2000hrs for 40°C, were compared. **UV!** absorbances at 600 nm and 650 nm were characteristic of the **SB59!** dye used to indicate the presence of NO_x, released by the denitration of **NC!** (figure **??**). The isosbestic point iden-

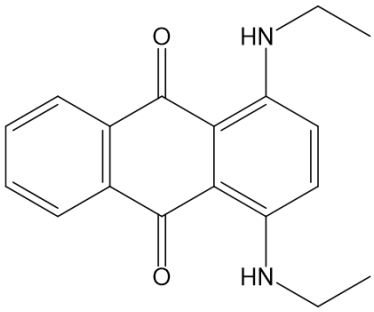

Figure 1.1: SB59! (**SB59!**) used to probe the release of nitrates from **NC!** using **UVVis!** (**UVVis!**) and ^{1}H NMR spectroscopy [**?**]. The action of nitrate absorption by the dye imitates that of stabilisers commonly used with nitrate ester formulations.

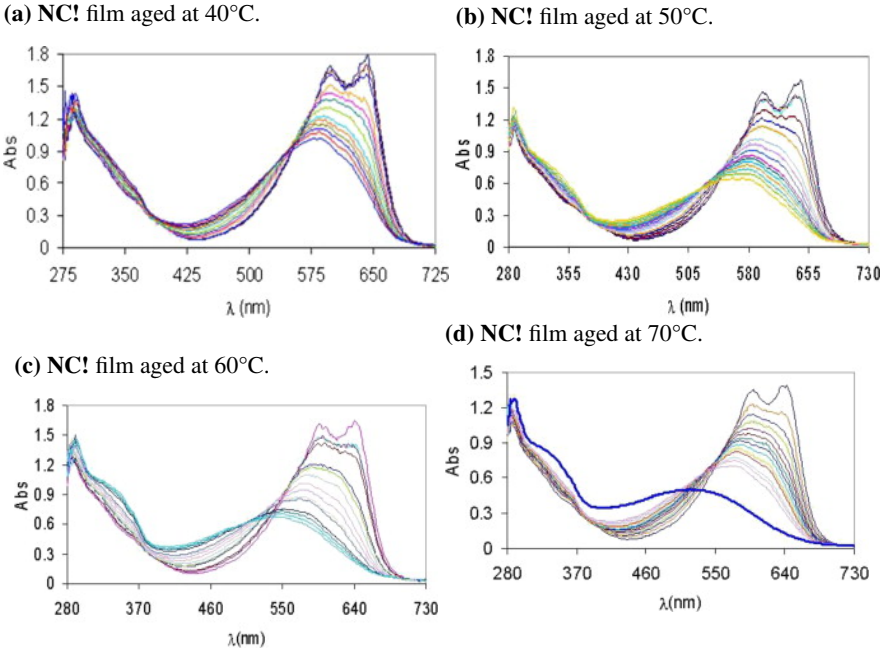

Figure 1.2: UVVis! spectra of aged **NC!**-based film, from the work of Moniruzzaman *et al.*[**?**]. The peaks at 600 nm and 650 nm are attributed to the π - π* transitions in the anthraquinone dye (**SB59!**). Spectral lines with highest absorbance peaks in this region correspond to the sample prior to heat treatment. Peaks below 400 nm indicate the formation of **SB59!** derivatives due to secondary reactions.

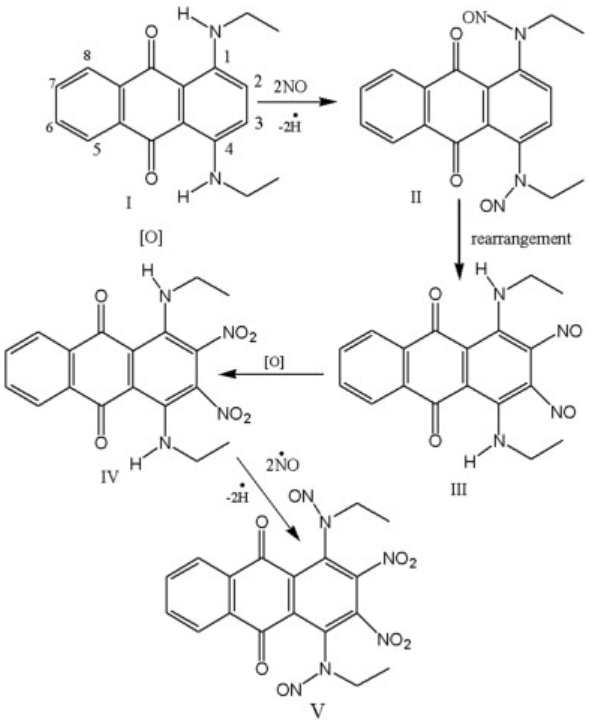

Figure 1.3: Proposed pathway for the reaction of **SB59!** dye with ·NO released as a result of denitration of **NC!** [**?**].

tified at 552 nm showed a proportional relationship between the concentration of **SB59!** as it decreased, with the concentration of the [**SB59! + NC!**] product as it increased. Samples exposed to higher ageing temperatures presented spectra dominated by products formed *via* secondary reactions. For samples aged at temperatures >40°C, the isosbestic point demonstrated a downwards shift with increasing dye consumption. In the case of the 70°C treated run, the final measurement (indicated by the royal-blue line in bold in figure **??**)) deviated from the isosbestic point entirely, with more than 81% consumption of the original dye concentration. The drift from the isosbestic point, in addition to the appearance of new absorbance peaks below 400 nm, allude to the presence of new species in the reaction mixture not generated by the primary reaction of **SB59!** and **NC!**. It is likely that these arise from the continued reaction of **SB59!** derivatives with **NC!** degradation products, or further derivatives thereof, as suggested in figure **??**. Following cleavage of the nitrate ester via homolytic fission, elimination of nitrous acid, or hydrolysis, the resulting residues available for further reaction with the polymer or other free molecules in the system. In the study of **PETN!** (**PETN!**) ageing at high temperatures (115°C - 135°C) in vacuum, and low temperatures (20°C - 65°C) in acetonitrile solution, Shepodd *et al.* commented that thermolysis produced a more complex and varied mixture, due to deeper degradation and recombination

Scheme 1.1: Thermolytic initiation

$$\mathrm{R{-}ONO_2} \longrightarrow \mathrm{R{-}O^{\cdot}} + {}^{\cdot}\mathrm{NO_2} \tag{1.1}$$

Propagation

$$\begin{aligned}\mathrm{R{-}O^{\cdot}} + {}^{\cdot}\mathrm{NO_2} \xrightarrow{\mathrm{R{-}ONO_2}} \mathrm{R{-}ONO_2} + {}^{\cdot}\mathrm{NO} + {}^{\cdot}\mathrm{NO_2} + \mathrm{N_2O_4} \\ + \mathrm{H_2O} + \mathrm{N_2O} + \mathrm{CO_2} + \mathrm{CO} \\ + \mathrm{C_2H_2O} + \text{other organic fragments}\end{aligned} \tag{1.2}$$

$$2\,{}^{\cdot}\mathrm{NO} + \mathrm{O_2} \longrightarrow 2\,{}^{\cdot}\mathrm{NO_2} \tag{1.3}$$

$$2\,{}^{\cdot}\mathrm{NO_2} \rightleftharpoons \mathrm{N_2O_4} \tag{1.4}$$

Scheme 1.2: Hydrolytic initiation

$$\mathrm{R{-}ONO_2 + H_2O} \longrightarrow \mathrm{R{-}OH + HNO_3} \tag{1.5}$$

$$\mathrm{R{-}OH + HNO_3} \longrightarrow \mathrm{R{=}O + HNO_2 + H_2O} \tag{1.6}$$

Propagation

$$\mathrm{HNO_3 + HNO_2} \rightleftharpoons \mathrm{N_2O_4 + H_2O} \tag{1.7}$$

$$\mathrm{N_2O_4} \rightleftharpoons 2\,{}^{\cdot}\mathrm{NO_2} \tag{1.8}$$

$$\mathrm{R{-}OH} + {}^{\cdot}\mathrm{NO_2} \longrightarrow {}^{\cdot}\mathrm{R{-}OH} + \mathrm{HNO_2} \tag{1.9}$$

$${}^{\cdot}\mathrm{R{-}OH + HNO_3} \longrightarrow \mathrm{R{=}O + H_2O} + {}^{\cdot}\mathrm{NO_2} \tag{1.10}$$

of radicals [**?**]. By contrast, the low temperature hydrolytic process emphasised formation of **PETRIN!** (**PETRIN!**) followed by side reactions with reduced likelihood of radical recombination in solution compared to in a solid, as $\bullet NO_2$ would be more likely to diffuse and react elsewhere. Chin *et al.* proposed schemes for the propagation of secondary reactions initated by both the thermolysis (scheme **??**) and hydrolysis of nitrate esters (scheme **??**) [**?**].

Termination reactions were not emphasised in either of the schemes for these cases. The hydrolysis scheme was adapted from an earlier work by Camera *et al.* involving the ni-

Scheme 1.3: Hydrolysis scheme for ethyl nitrate

$$\mathrm{CH_3CH_2ONO_2 + H^+} \overset{\text{fast}}{\rightleftharpoons} \mathrm{CH_3CH_2ONO_2H^+} \tag{1.11}$$

$$\mathrm{CH_3CH_2ONO_2H^+} \overset{\text{slow}}{\rightleftharpoons} \mathrm{CH_3CH_2OH + {NO_2}^+} \tag{1.12}$$

$$\mathrm{{NO_2}^+ + 2\,H_2O} \overset{\text{fast}}{\rightleftharpoons} \mathrm{HNO_3 + H_3O^+} \tag{1.13}$$

trate ester decomposition and subsequent reactions of **EN!** (**EN!**) (where R = CH_3CH_2 for the scheme above) [**?**]. The original study included an expansion of the hydrolysis step (equation **??**), where the involvement of NO_2^+ was illustrated (scheme **??**).

It was highlighted by Camera, that the oxidation of alcohol by nitric acid (equation **??**) is slow and thus rate-limiting. The mechanism is likely to occur *via* a series of intermediate reactions of which the details are not known. Following the generation of nitrous acid, subsequent oxidations occur rapidly. According to Rigas *et al.*, alcohols are more susceptible to wet oxidation than esters [**?**]. A higher concentration of unsubstituted hydroxyl groups in the system, and therefore a fewer nitrate ester groups (or a lower **DOS!** (**DOS!**) value), decreases overall stabililty.

Equations **??** - **??** describe a possible branched radical chain mechanism, fed by the nitrous and nitric acids produced during the hydrolysis and alchohol oxidation reactions during the initiation stage. By contrast, the propagation reactions in the branched radical chain mechanism for thermolysis are poorly characterised (equation **??**), defined only by the observable products. This is likely due to their rapid and varied nature, rendering it difficult to follow spectroscopically.

Aellig *et al.* presented an alternative scheme for the decomposition of benzyl nitrate (R = $PhCH_2$), involving more interaction with the solvent [**?**]:

Both the Camera/Chin and Aellig schemes above produce final end products observed in

Scheme 1.4: HNO_3 decomposition initiation

$$4\,HNO_3 \rightleftharpoons 4\,^{\cdot}NO_2 + 2\,H_2O + O_2 \tag{1.14}$$

$$2\,^{\cdot}NO_2 + H_2O \rightleftharpoons N_2O_4 + H_2O \tag{1.15}$$

$$N_2O_4 + H_2O \longrightarrow HNO_3 + HNO_2 \tag{1.16}$$

Propagation

$$R{-}OH + HNO_2 \rightleftharpoons R{-}ONO + H_2O \tag{1.17}$$

$$R{-}ONO \longrightarrow R{=}O + HNO \tag{1.18}$$

$$^{\cdot}NO_2 + HNO \longrightarrow HNO_2 + ^{\cdot}NO \tag{1.19}$$

$$2\,^{\cdot}NO + O_2 \longrightarrow 2\,^{\cdot}NO_2 \tag{1.20}$$

Termination

$$2\,HNO \longrightarrow HON{=}NOH \tag{1.21}$$

$$HON{=}NOH \longrightarrow N_2O + H_2O \tag{1.22}$$

the decomposition of **NC!**. In particular, Aellig's scheme accounts for the production of N_2O, which forms a significant part of the decomposition eluent [**?**]. Whilst the schemes do not a propose an exhaustive description of the full spectrum of reactions that take place in the **NC!** matrix during its slow ageing, the early stage reactions of the key species responsible for decomposition are encapsulated.

It is widely agreed that first-stage decomposition follows a first-order process (or pseudo-first order, with respect to hydrolysis reactions). A number of studies observe catalytic rate of decay for the longer-term aging processes. Dauerman [**?**] observed that when **NC!** was treated with NO_2 gas before heating, the time required for sample ignition halved. He suggested that the NO_2 adsorbed onto the surface acted as a catalysing agent.

Neutral and alkaline hydrolysis reactions follow a pseudo-first order process, however it has been suggested that the presence of acid facilitates a catalytic rate of degradation after an initial incubation period. Multiple studies have addressed the decomposition reactions of nitrate esters following the initial scission of the nitrate group [**?**, **?**, **?**, **?**, **?**] In their work looking into the atmospheric reactions of methynitrate and methylperoxy nitrate Arenas suggested it was possible for the homolytic denitration reaction of methynitrate to share a common peroxy intermediate with the peroxide [**?**]. This could account for some of the lower order NO_x generated. In this section, secondary and extended reaction schemes for the low temperature ageing of **NC!** are explored. Decomposition pathways defined by Chin, Camera and Aellig *et al.* are probed to determine the reactions responsible for the experimentally observed degradation products. The reactions found to be energetically feasible from the proposed routes will be scrutinised to determine whether an autocatalytic pathway can be formed from the thermodynamically validated reaction schemes.

1.2 Methodology

The schemes proposed by Chin, Camera and Aellig *et al.* were used to construct possible degradation routes for **NC!** with the products of homolytic fission, elimination of HNO_2 and acid hydrolysis used as the starting point. Pathways were constructed based on propagation of the given reactions in a step-wise fashion; subsequent reactions were dependent on the products generated in preceding steps. An abundance of water and oxygen were assumed present in the system, attributed to air exposure under the wetted storage conditions of **NC!**. Unsubsitutued alcohol moieties (R-OH) were also presumed available, due to incomplete nitration during the synthesis of **NC!** [**?**], and re-generation following denitration *via* hy-

drolysis. The schemes were modelled with **EN!**, then expanded to the **NC!** monomer. Free energies of reaction (Δ G) were used to determine the feasibility of each reaction.

1.2.1 Computational details

All geometry optimisations were conducted in **G09!** (**G09!**), using the **wb97xd!** and **B3LYP!** functionals. Optimisations and thermochemistry calculations were performed to the level of 6-31+G(2df,p) with tight convergence criteria (table **??**). Calculations were performed in both vacuum and with **PCM!** (**PCM!**) to introduce implicit solvent effects. Chemical species were constructed using **GView!** (**GView!**) and for molecules of more than 3 atoms, the "Clean" function was used to re-order atoms to a preliminary starting geometry. Energies of optimised structures were checked against values listed on NIST Computational Chemistry Comparison and Benchmark Database [**?**] if analogous molecules to a similar level of theory were available.

1.3 Results and Discussion

Simplified schemes for the possible ageing reactions of nitrate esters beginning from homolytic fission, elimination of HNO_2 or acid hydrolysis are illustrated in schemes **??** - **??**. When starting with the products of homolytic fission, a branched radical chain mechanism dominates. $\bullet NO_2$ and HNO_2 were consumed and regenerated, supporting the theory that these may be species contributing to the observed autocatalytic rate of decomposition, following a first-order rate induction period [**?**, **?**, **?**]. For all schemes, R=O and N_2O were terminating species. Whilst $N_2O$is released into the environment, R=O remains in the system may go on to participate in further decomposition reactions leading to ring opening. The protonation site of **EN!** was inspected to determine whether it matched that of the hydrolytic denitration of **NC!**, therefore following the same extended hydrolysis scheme.

Table 1.1: Free energies of protonation for each oxygen site on **EN!**.

Protonated site		ΔG_r /kcal mol^{-1}			
		wb97xd!	PCM	**B3LYP!**	PCM
Terminal (upper)	$CH_3CH_3ONO_2H^+$	−12.28	8.82	−13.78	5.63
Terminal (lower)	$CH_3CH_3ONO_2H^+$	−9.48	9.46	−11.13	5.65
Bridging	$CH_3CH_3O(H^+)NO_2$	−9.32	9.06	−15.31	6.67

Table **??** shows the protonation energies for the three different oxygen sites on **EN!**. Despite the upper terminal oxygen possessing the most thermodynamically favourable en-

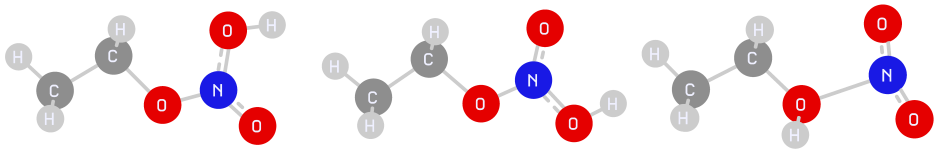

(a) Upper terminal oxgen. Bond(O–NO_2): 1.28 Å

(b) Lower terminal oxgen. Bond(O–NO_2): 1.28 Å

(c) Bridging oxgen. Bond(O–NO_2): 1.98 Å

Figure 1.4: Optimised geometries of the possible protonation sites on **EN!**.

ergy of protonation, inspection of the reaction geometries shows that the bridging structure most resembles that expected for the liberation of the NO_2^+ group at the next step. Though appearing less thermodynamically favourable when compared to protonation at the terminal upper oxygen site, the higher energy of reaction likely arises from the instability of the protonated complex. The elongation of the $O-NO_2$ bond allows stabilisation of the proton at the bridging site, faciliting the facile departure of NO_2^+. Subsequent calculations involving the energy of the protonated **EN!** will employ the values associated with the protonated bridging site.

Table **??** shows the energies for the reactions in all schemes, for both **EN!** and the **NC!** monomer.

The **wb97xd!** (**wb97xd!**) values obtained for the formation of N_2O_4 from $2{\bullet}NO_2$ are in good agreement with the experimentally recorded value of -1.4 kcal mol^{-1} [**?**, **?**]. It is noted that the **B3LYP!** (**B3LYP!**) result does not perform so well for this reaction. This may arise from a number of factors, including the limitation to short-range interactions in **B3LYP!**, or the geometry optimisation procedure, whereby a small variation or imperfect minimisation in the obtained optimised structures for the reaction species is amplified in the calculation of reation energies. Comparison of reaction energies for **EN!** and the monomer shows that most processes are more thermodynamically favourable in the case of **NC!**.

1.4 Summary

A number of proposed reactions following the denitration of **NC!** were validated by calculating energies of reaction with the **wb97xd!** and **B3LYP!** methods.It as found that except in the case nitric acid decomposition, $4\,HNO_3 \rightleftharpoons 4\,NO_2 + 2\,H_2O + O_2$, most reactions were feasible at atmospheric conditions. The reactions were used to create rough schemes of the possible routes degradation routes, with increasing number of the **NC!** decay. It can be seen that it is the NO_2 species driving oxidation in all three schemes, and plays a central

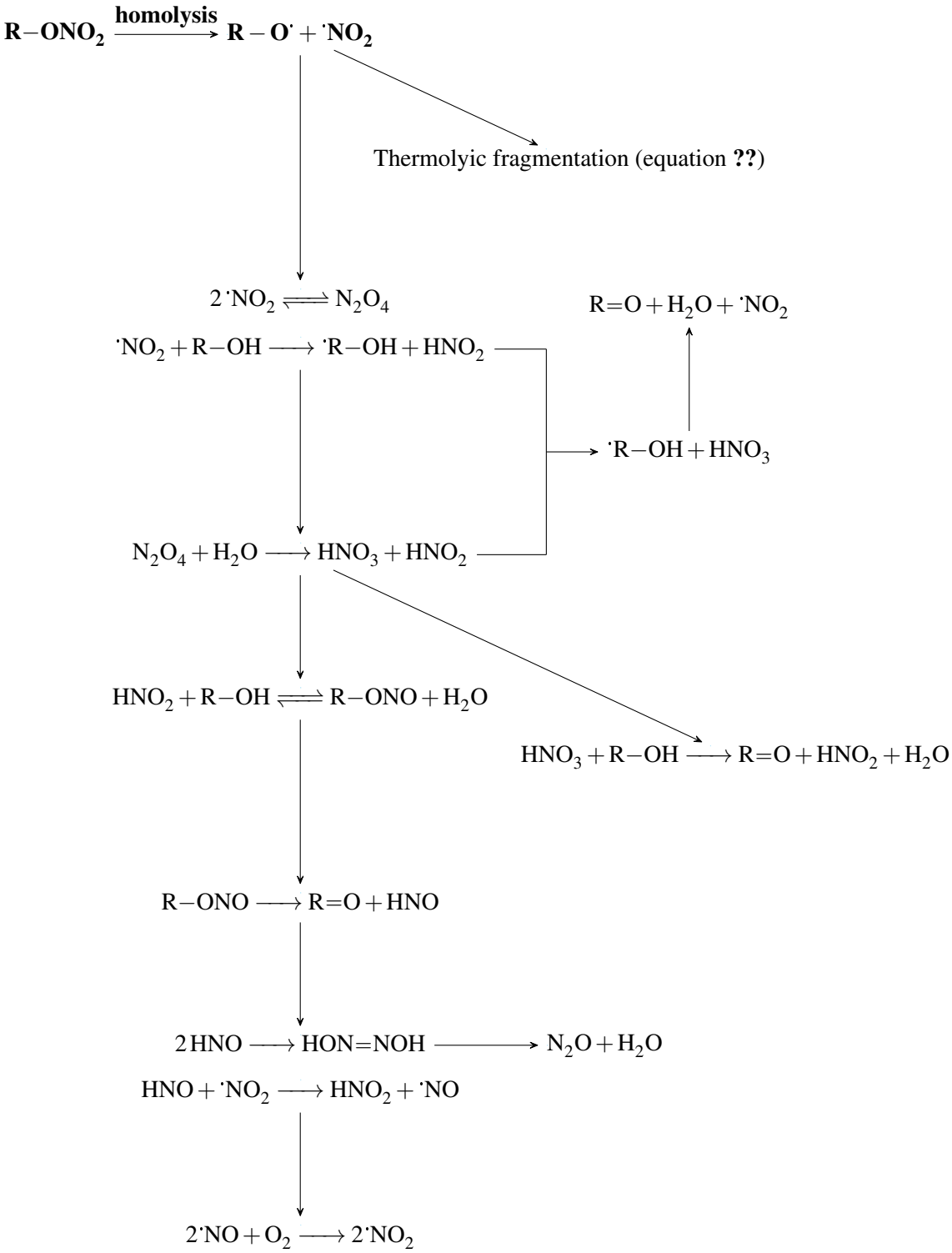

Scheme 1.5: Proposed degradation pathway starting from the homolytic fission of the nitrate ester, derived from the schemes presented by Camera [**?**] and Aellig[**?**].

Table 1.2: Energies of nitrate ester decomposition reactions proposed by Camera [**?**], Chin [**?**] and Aellig [**?**]. R = CH_3CH_2 for **EN!**, and R = $(H_3CO)_2C_6H_9O_3$ (bi-methoxy capped glucopyraonse monomer unit).

Reaction	ΔG_r /kcal mol^{-1}			
	wb97xd!	PCM	**B3LYP!**	PCM
$N_2O_4 + H_2O \longrightarrow HNO_3 + HNO_2$	2.25	1.85	5.13	4.18
$N_2O_4 \rightleftharpoons 2\,^{\cdot}NO_2$	0.12	1.46	−0.54	−0.16
Radical reactions				
$^{\cdot}NO_2 + HNO \longrightarrow HNO_2 + {}^{\cdot}NO$	−28.22	−28.67	−27.33	−27.63
$2\,^{\cdot}NO + O_2 \longrightarrow 2\,^{\cdot}NO_2$	−20.77	−21.97	−21.16	−22.16
Acid reactions				
$HNO_3 + HNO_2 \rightleftharpoons N_2O_4 + H_2O$	−2.25	−1.85	−5.13	−4.18
$4\,HNO_3 \rightleftharpoons 4\,^{\cdot}NO_2 + 2\,H_2O + O_2$	53.35	58.36	42.61	46.94
$2\,HNO \longrightarrow HON{=}NOH$	−38.97	−39.72	−36.63	−37.41
$HON{=}NOH \longrightarrow N_2O + H_2O$	−48.08	−48.18	−50.55	−50.75
Ionic reactions				
$NO_2^+ + 2\,H_2O \rightleftharpoons HNO_3 + H_3O^+$	−0.90	−1.34	1.77	2.46
EN! (R = CH_3CH_2)				
$R{-}ONO_2 + H_2O \longrightarrow R{-}OH + HNO_3$	4.56	5.24	4.00	4.86
$R{-}OH + HNO_3 \longrightarrow R{=}O + HNO_2 + H_2O$	−34.06	−38.43	−37.59	−41.77
$R{-}OH + {}^{\cdot}NO_2 \longrightarrow {}^{\cdot}R{-}OH + HNO_2$	16.38	13.92	15.89	13.70
$^{\cdot}R{-}OH + HNO_3 \longrightarrow R{=}O + H_2O + {}^{\cdot}NO_2$	−50.44	−52.35	−53.48	−55.47
$R{-}OH + HNO_2 \rightleftharpoons R{-}ONO + H_2O$	−3.21	−3.28	−2.64	−2.95
$R{-}ONO \longrightarrow R{=}O + HNO$	−1.50	−5.82	−4.37	−8.50
NC! monomer (R = $(H_3CO)_2C_6H_9O_3$)				
$R{-}ONO_2 + H_2O \longrightarrow R{-}OH + HNO_3$	0.68	5.63	0.61	−0.70
$R{-}OH + HNO_3 \longrightarrow R{=}O + HNO_2 + H_2O$	−36.73	−38.34	−41.71	−41.70
$R{-}OH + {}^{\cdot}NO_2 \longrightarrow {}^{\cdot}R{-}OH + HNO_2$	14.71	11.15	13.03	23.21
$^{\cdot}R{-}OH + HNO_3 \longrightarrow R{=}O + H_2O + {}^{\cdot}NO_2$	−51.44	−49.49	−54.75	−56.37
$R{-}OH + HNO_2 \rightleftharpoons R{-}ONO + H_2O$	−4.43	−7.30	−4.31	−0.18
$R{-}ONO \longrightarrow R{=}O + HNO$	−2.93	−1.71	−6.82	−11.21

role in the extended degradation scheme of **NC!**.

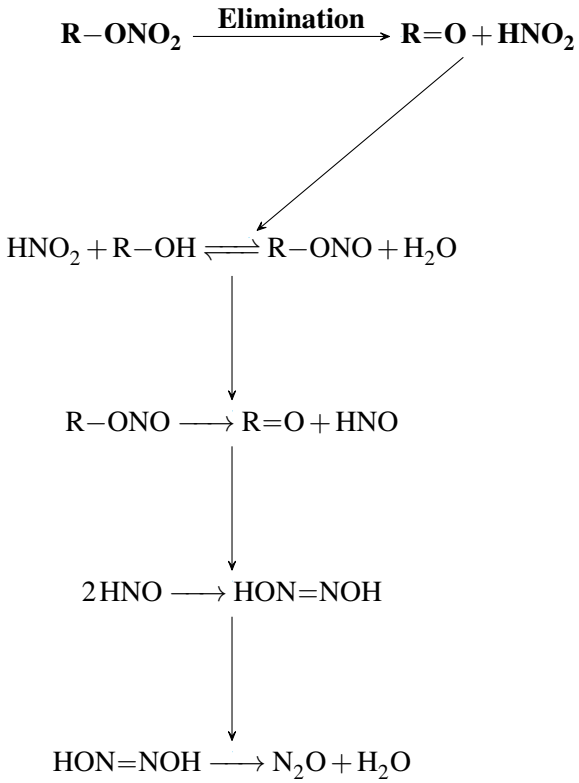

Scheme 1.6: Proposed degradation pathway starting from the elimination of HNO_2 from a nitrate ester, derived from the schemes presented by Camera [**?**] and Aellig[**?**].

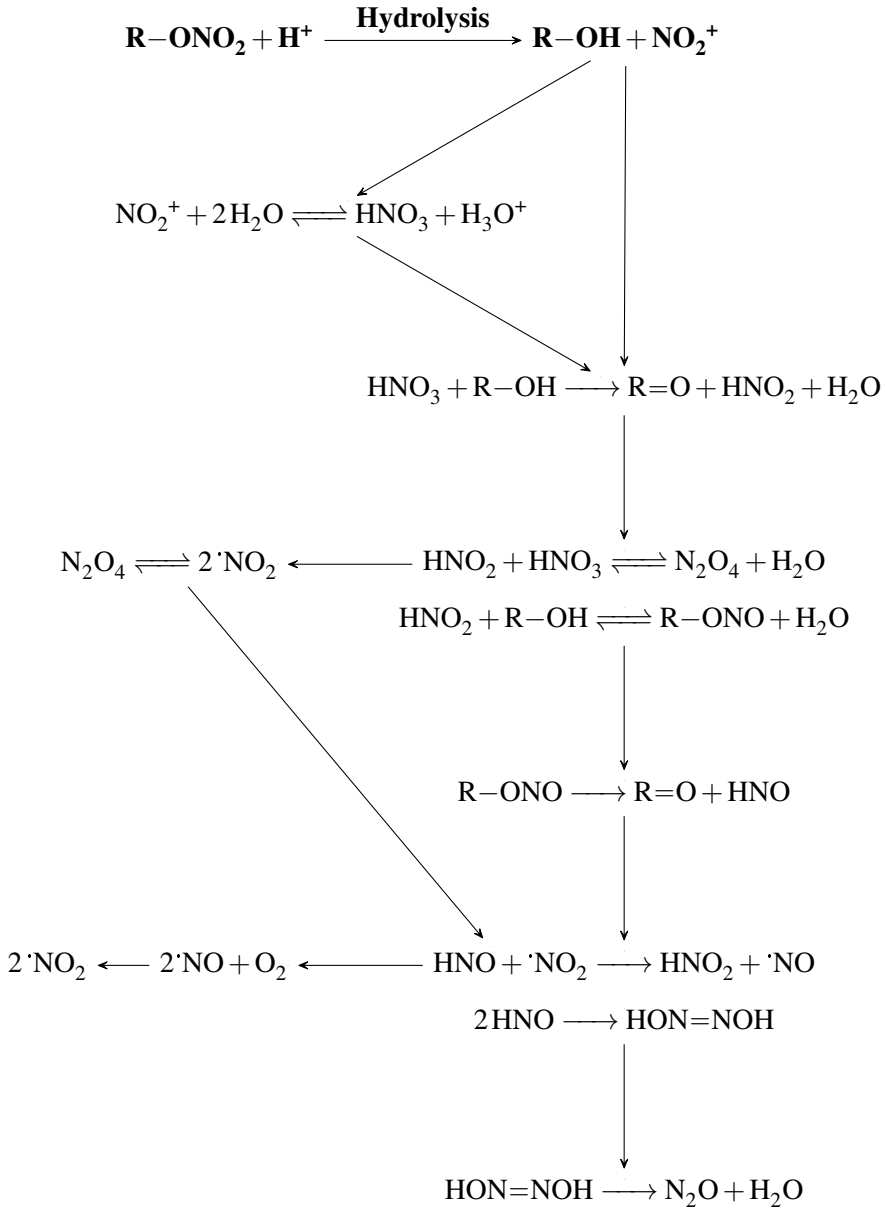

Scheme 1.7: Proposed degradation pathway starting from the acid hydrolysis of a nitrate ester, derived from the schemes presented by Camera [**?**] and Aellig[**?**].